Summertime carbonaceous aerosols collected in the marine boundary layer of the Arctic Ocean

Zhouqing Xie,[1,2] Joel D. Blum,[3] Satoshi Utsunomiya,[3] R. C. Ewing,[3] Xinming Wang,[4] and Liguang Sun[1]

Received 1 March 2006; revised 18 July 2006; accepted 11 August 2006; published 27 January 2007.

[1] The chemistry, morphology, and microscale to nanoscale structures of carbonaceous aerosols from the marine boundary layer of the Arctic Ocean were investigated by a variety of electron microscopy techniques, including scanning electron microscopy (SEM), high-resolution transmission electron microscopy (HRTEM), and energy-dispersive X-ray spectroscopy (EDS). The relative levels of particles of black carbon (BC) were determined by electron paramagnetic resonance (EPR). Polycyclic aromatic hydrocarbons (PAHs) absorbed onto BC particles were extracted by the soxhlet extraction method and analyzed by gas chromatography mass spectrometry (GC-MS). The results show that the dominant particles of BC are char particles with spherical shape, porous structure, and high sulfur content, which are typically derived from residual oil combustion on ships. The spatial distribution of BC from ship emissions was found to be concentrated around the periphery of the Arctic Ocean, suggesting relatively intensive contamination by ships in the Russian and Canadian Arctic. The abundance of PAHs on BC particles ranges from 142 to 2672 pg/m^3 (mean = 702 pg/m^3), which is significantly higher than values previously measured by land-based observation. Thus we find that ship emissions are a potentially important contributor to the PAH levels at some locations in the Arctic Ocean during the summer.

Citation: Xie, Z., J. D. Blum, S. Utsunomiya, R. C. Ewing, X. Wang, and L. Sun (2007), Summertime carbonaceous aerosols collected in the marine boundary layer of the Arctic Ocean, *J. Geophys. Res.*, *112*, D02306, doi:10.1029/2006JD007247.

1. Introduction

[2] Carbonaceous particles in the atmosphere, because of their chemical and physical properties, play an important role in the Earth's radiation budget [*Charlson et al.*, 1992; *Haywood and Ramaswamy*, 1998], health effects from air pollution [*Douglas et al.*, 1993; *Pope III et al.*, 1999], and tropospheric chemistry [*Chughtai et al.*, 1999; *Kirchner et al.*, 2000]. Carbonaceous particles are mainly derived from incomplete combustion of fossil fuels and biomass [*Chen et al.*, 2005]. There are two main forms including light-absorbing black carbon (BC) and light-scattering organic carbon (OC) [*Chen et al.*, 2005; *Novakov et al.*, 2005]. Black carbon is a randomly formed particulate carbon that, in addition to carbon atoms arranged in an aromatic framework, contains many varieties of OC that together comprise an extremely complex system [*Yordanov et al.*, 2001; *Fernandes et al.*, 2003; *Fernandes and Brooks*, 2003]. Many OC compounds, such as polycyclic aromatic hydrocarbons (PAHs), are embedded within the pore structure of BC or adsorbed onto its surface from the gas phase [*Yordanov et al.*, 2001]. The annual global emissions of BC have been estimated at 12–24 Tg/yr [*Penner et al.*, 1993; *Cooke and Wilson*, 1996].

[3] BC has been implicated in previous studies as potentially affecting Arctic climate via alteration of the atmospheric temperature profile, cloud temperature and amount, the tropopause height, and for accelerating polar ice melting [*Clarke and Noone*, 1985; *Hansen et al.*, 1997; *Ackerman et al.*, 2000; *Hansen and Nazarenko*, 2004; *Koch and Hansen*, 2005; *Xie et al.*, 2005]. Black carbon particles are commonly believed to be transported to the Arctic during the winter and spring via 'Arctic haze' transport events [*Shaw*, 1995]. More detailed analyses using atmospheric chemical signatures [*Rahn and Lowenthal*, 1984; *Lowenthal and Rahn*, 1985; *Lowenthal and Borys*, 1997] and considering air mass trajectory information [*Cheng et al.*, 1993] suggests Eurasia as the primary source of the winter-spring Arctic haze. Recently, *Koch and Hansen* [2005] argued that the predominant sources of Arctic BC today are from south Asian industrial and biofuel emissions (30%) and biomass burning (28%), with slightly more than half of the biomass coming from north of 40°N. Long-range transport of

[1] Institute of Polar Environment, School of Earth and Space Sciences, University of Science and Technology of China, Hefei, Anhui, China.
[2] Formerly at Department of Geological Sciences, University of Michigan, Ann Arbor, Michigan, USA.
[3] Department of Geological Sciences, University of Michigan, Ann Arbor, Michigan, USA.
[4] State Key Laboratory of Organic Geochemistry, Guangzhou Institute of Geochemistry, Chinese Academy of Sciences, Wushan, Guangzhou, China.

0148-0227/07/2006JD007247

anthropogenic sources thus appears to dominate the Arctic sources of BC.

[4] During the Second Chinese Arctic Research Expedition (July–September 2003), aerosols were collected onboard a ship in the marine boundary layer. In a previous report based on the same sampling expedition, the sources of inorganic chemical components were determined on the basis of factor analysis using synchrotron radiation X-ray fluorescence (SR-XRF) [*Xie et al.*, 2006]. The results suggested that ship emissions may significantly contribute to air pollution in the marine boundary of the Arctic Ocean in summer, implying a potential source of BC in this region that has not received much previous attention. Investigation of carbonaceous particles in these samples provides an opportunity to understand BC contamination from ship emissions in the "real world." Various electron microscopy techniques, including scanning electron microscopy (SEM), high-resolution transmission electron microscopy (HRTEM), and energy-dispersive X-ray spectroscopy (EDS) were applied to measure the morphology, microstructure, and composition of individual carbonaceous particles. The levels of BC were determined by the electron paramagnetic resonance (EPR) technique. Polycyclic aromatic hydrocarbons (PAHs) absorbed onto BC particles were extracted by the traditional soxhlet extraction method and analyzed by gas chromatography mass spectrometry (GC-MS).

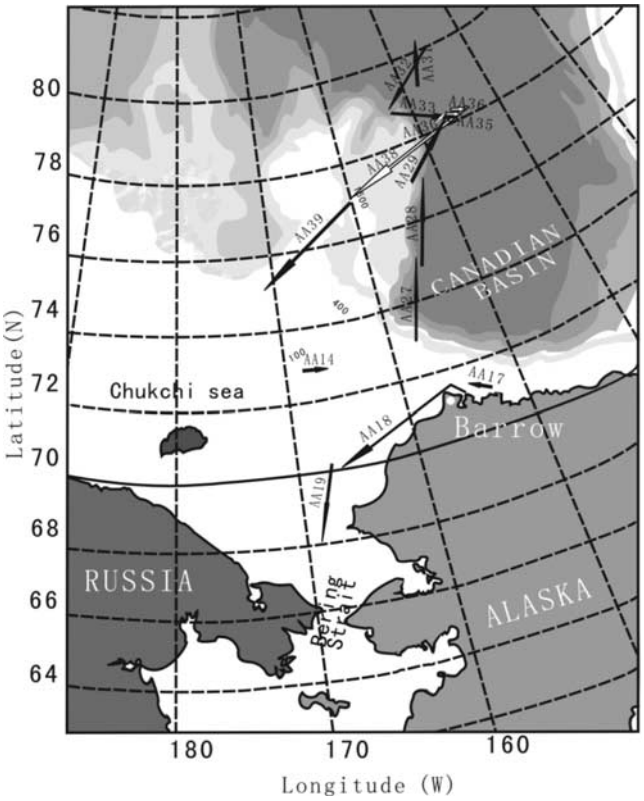

Figure 1. Sampling locations along ship tracks in the Arctic Ocean.

2. Experimental Methods

2.1. Sample Collection

[5] The procedure for aerosol collection was described in detail in our previous paper [*Xie et al.*, 2006]. Briefly, total suspended particle (TSP) samples were collected aboard the Chinese Arctic and Antarctic Administration (CAAA) R/V *Xuelong* during the Second Chinese Arctic Research Expedition (July–September 2003) using a high-volume bulk aerosol sampler (Tianhong Instruments, Wuhan, China) and Whatman 41 cellulose filters [*Xie et al.*, 2002]. Other recent studies have also measured PAHs and/or soot in airborne particulate matter using cellulose filters [*Crimmins et al.*, 2004; *Ochsenkuhn-Petropoulou et al.*, 2003]. The same samples selected for SR-XRF measurement [*Xie et al.*, 2006] were also selected for analysis in this study; the sample locations are shown in Figure 1. One snow sample collected near Barrow, Alaska, in March 2005 was used for a comparative analysis.

2.2. Electron Microscopy

[6] SEM and HRTEM were conducted in the Electron Microanalysis Laboratory of the University of Michigan. A small piece (1 cm^2) was cut from the original filters and coated with carbon and/or gold for imaging by SEM. For HRTEM analysis, particles in the filters were extracted using an ultrasonic bath and centrifugation. Portions of the filters (1 cm^2) were cut into pieces and placed into 15 ml centrifuge tubes. Five ml of deionized water was added to each tube and they were sonicated for one hour. The filters were then removed and a TEM copper grid coated with carbon mesh was put into the bottom of the tube. The solution was centrifuged for one hour (at 2500 rpm) with the copper grid in place. Carbonaceous particles were deposited on the surface of the carbon mesh, which was then used for HRTEM observation. The snow sample was melted in a centrifuge tube. A TEM copper grid coated with carbon mesh was placed into the bottom of the tube and it was centrifuged for one hour (at 2500 rpm). The grid was then used for HRTEM observation. The details of the electron microscopy measurements have been described previously [*Utsunomiya and Ewing*, 2003].

2.3. Electron Paramagnetic Resonance (EPR)

[7] The EPR spectra were recorded on a JEOL JES-FA200 spectrometer operating in the X-band at the Structure Research Laboratory of the University of Science and Technology of China. A small portion of each filter (1 cm^2) was subsampled and placed in a quartz tube. The measurements were performed using a standard cavity with a computer-interfaced spectrometer, and all measurements were performed at room temperature (300K). The microwave power was kept constant at 1mW, and the magnetic field modulation amplitude was 8G. Fifteen samples and one blank filter were measured. The uncertainty of the data is less than 5% [*Yordanov et al.*, 1996, 2001; *Yordanov and Najdenova*, 2004].

2.4. PAHs Analysis

2.4.1. Sample Extraction

[8] A mixture of deuterated PAH standards (naphthalene-d8, acenaphthene-d10, phenantgrene-d10, chrysene-d12, and perylene-d12) was added to all of the samples as surrogate compounds, and then a 72 h Soxhlet extraction was carried out with redistilled dichloromethane. The

extracts were concentrated and solvent exchanged with redistilled hexane, and then purified using a 1:2 alumina/silica column chromatography. The first fraction, containing aliphatic hydrocarbons, was eluted with 30 ml of hexane. The second fraction, containing PAHs, was collected by eluting 70 ml of DCM/hexane (3:7 v/v) and then concentrated to a final volume of 200 μl under a gentle stream of nitrogen. Eight microliters of 50 μg/ml of hexamethylbenzene (Aldrich Chemicals, Gillingham, Dorset, United Kingdom), was added to the samples as an internal standard before instrumental analysis.

2.4.2. Instrumental Analysis and Parameters

[9] PAHs were analyzed using an Agilent 6890 series gas chromatograph/5973 mass spectrometric detector in the selective ion monitoring (SIM) mode with a 50 m HP-5 capillary column (i.d.0.32 mm, 0.17 μm film thickness). The column temperature was initiated at 80°C (held for 2 min) and increased to 290°C at 4°C/min (held for 30 min). The limit of detection, defined as a signal of three times the noise level and calculated using the average sampling volume (2051 m^3), ranged from 0.6 pg/m^3 for acenaphthylene to 7.0 pg/m^3 for coronene.

2.4.3. Quality Control/Quality Assurance

[10] Three field blanks and six laboratory blanks were extracted and analyzed in the same way as field samples. There was no difference between concentrations of analytes in the laboratory and field blanks, indicating contamination was minimal during sampling, transport, and storage. Surrogate recoveries (both field and laboratory samples) were 75 ± 21% for naphthalene-d8, 87 ± 15% for acenaphthene-d10, 98 ± 15% for phenanthrene-d10, 90 ± 16% for chrysene-d12, and 84 ± 16% for perylene-d12, respectively. The relative differences for individual PAHs in paired duplicate samples (n = 3) were all <15%. Recoveries of PAHs in spiked blank samples (PAH standards spiked into solvent with clean filters), matrix spiked samples (PAH standards spiked into preextracted filters), and National Institute of Standards and Technology (NIST, Gaithersburg, MD) 1941 reference samples (n = 3) ranged from 77 to 104%, 72 to 98%, and 80 to 120%, respectively. The reported results were not recovery corrected. The PAH experiments was conducted at the State Key Laboratory of Organic Geochemistry of the Chinese Academy of Sciences.

3. Results and Discussion

3.1. Morphologies, Microstructure, and Elemental Compositions

[11] Micrographs of carbonaceous particles are shown in Figures 2a and 2b. The particles are dominated by spherical primary particles with an obvious porous structure, and a size range from sub-μm to μm. Carbon cenospheres with porous surfaces are very typical of char particles derived from residual oil combustion, which have quite different morphologies as compared with those of soot aggregates and other carbonaceous particles [*Chen et al.*, 2005]. Soot particles were observed to cover the surface of the char particles (Figure 2b). The morphological differences among carbonaceous particles are mainly related to differences in their sources [*Fernandes et al.*, 2003] and formation conditions [*Chen et al.*, 2005]. For example, plant-derived BC shows very little aciniform carbon as compared with fossil fuel BC [*Fernandes et al.*, 2003]. Among the fossil fuel BC, primary soot particles are formed by generation of nuclei during condensation in cooling postcombustion gaseous streams. Relatively larger char particles, on the other hand, are derived from pyrolysis and oxidation of fuel particles. The nature of the fuel, the fuel/air ratio, and the temperature and duration of combustion all play a role in determining the morphology and crystallinity of these carbonaceous particles [*Chen et al.*, 2005; *Chughtai et al.*, 2002; *Jones et al.*, 2004]. The spherical shapes observed here reflect the nature of liquid fuel droplets and the lack of any crystalline phase in them [*Chen et al.*, 2005].

[12] An HRTEM image of a char particle and attached soot is shown in Figure 3a. These two kinds of particles are distinct. HRTEM images of soot aggregates show an onion-like structure, which has concentrically arranged carbon layers with a d-spacing corresponding to graphite but without longer-range periodicity [*Utsunomiya et al.*, 2002]. In contrast, char particles do not exhibit concentric structures. Instead, they typically exhibit a diffuse diffraction halo in the selected area electron diffraction (SAED) pattern that is characteristic of an amorphous solid (Figure 4). The structures of both the char particles and the soot attached to the char particles are different from the BC in the snow sample. In the latter case, the BC is derived from high-temperature combustion (Figure 3b), and the HRTEM image clearly reveals the graphite structure by the spacings of the continuous lattice fringes. BC occurrences in Arctic snow in spring were presumed to be related to "Arctic haze," which probably brings BC from anthropogenic sources at lower latitudes.

[13] The chemical composition of BC particles was analyzed using TEM/EDS. Figure 5 shows the typical EDS spectrum of char particles. Note that TEM specimens were not coated with carbon and EDS analyses were carried out on the samples sitting on the hole of a holey carbon mesh to avoid a contribution to the carbon signal from the mesh. Besides the dominant carbon, the S content is also quite significant. Sulfur K-edge X-ray absorption fine structure (XAFS) spectroscopy indicates that thiophene is the major organic sulfur form in residual oil fly ash (ROFA) [*Chen et al.*, 2004]. In addition, the particles were coated/mixed with carbonaceous phases containing transition metals (e.g., V), which is a typical characteristic of carbonaceous particles derived from residual oil combustion [*Chen et al.*, 2005].

[14] In brief, morphologies, microstructure and elemental compositions indicate that the dominant carbonaceous particles observed in the samples were char particles derived from residual oil combustion. This finding is in agreement with our previous report [*Xie et al.*, 2006] that the emissions from ships using residual oil play an important role in chemical compositions of aerosols.

3.2. Relative Levels of BC and Its Spatial Distribution

[15] Since samples were collected using cellulose filters, BC could not be determined by a thermal-optical carbon analyzer, which is now a common method [*Xie et al.*, 2005]. Thus electron paramagnetic spectroscopy was used to measure the levels of BC found in the filters. In previous studies, it was demonstrated that it is possible to study the

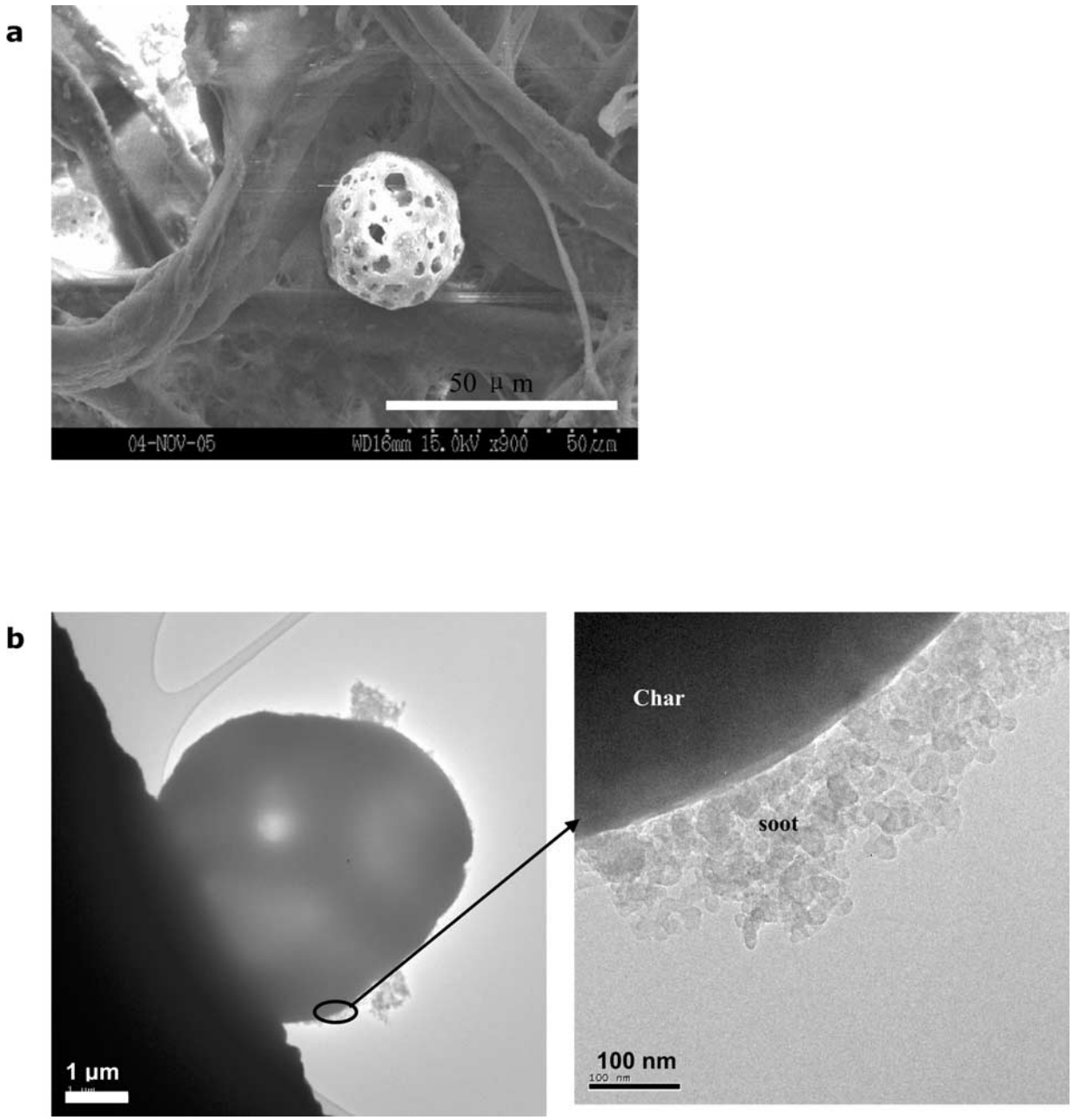

Figure 2. (a) Scanning electron microscopy (SEM) images of carbonaceous particles, which is spherical with porous surfaces; (b) transmission electron microscopy (TEM) images of carbonaceous particles, displaying soot covering the surface of char.

content of BC in aerosols using electron paramagnetic resonance (EPR) spectrometry [*Yordanov et al.*, 1996, 2001; *Yordanov and Najdenova*, 2004]. The applicability of EPR is based on the fact that BC is paramagnetic and PAHs absorbed onto the surfaces of BC are EPR "silent." The advantage of EPR is that it records only paramagnetic substances, and thus the estimates of BC content are rapid (~30 min) and unambiguous. In addition, because the method is nondestructive, samples can be retained for archival purposes and further study.

[16] A typical room temperature EPR spectrum of aerosol particles collected in the marine boundary layer and recorded with a broad magnetic field sweep is shown on Figure 6. The broad singlet signal with g = 2.0 corresponds to Fe and/or in part to Mn ions present in the particles. Other components like Si, Ca, Al, K, etc. are EPR silent. The relative levels of iron in each sample, which were obtained by synchrotron radiation X-ray fluorescence [*Xie et al.*, 2006], are also listed in Table 1. The narrow sharp singlet line (shown with an arrow on Figure 6) corresponds to the BC. Its EPR parameter is g = 2.0039, similar to values previously reported [*Yordanov et al.*, 1996, 2001; *Yordanov and Najdenova*, 2004]. The relative intensity of this line was monitored in the present study, indicating the relative

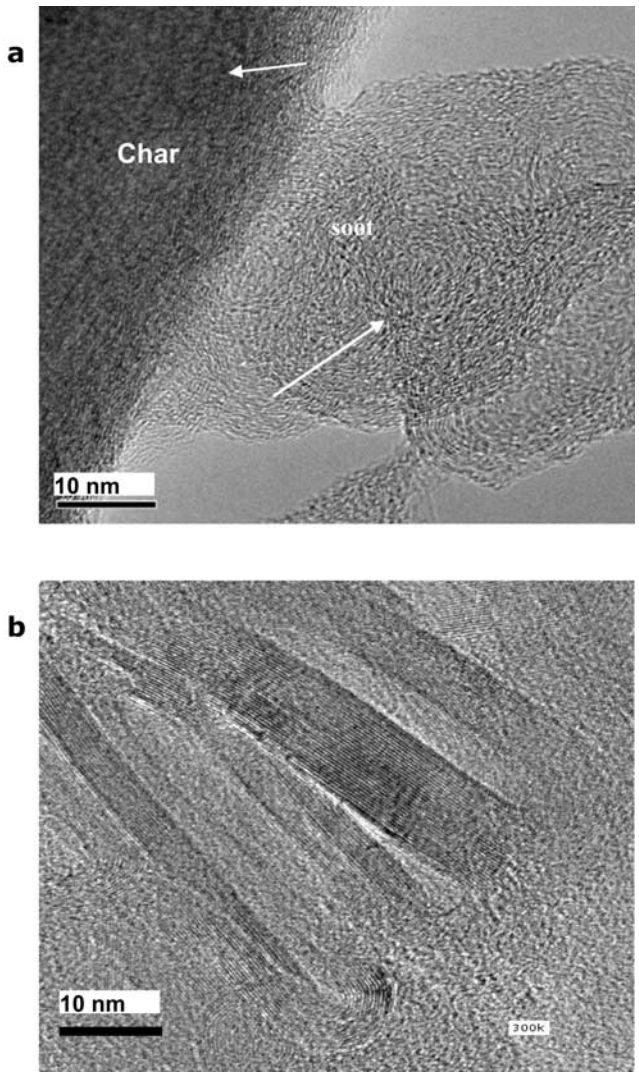

Figure 3. High-resolution TEM images of carbonaceous particles.

levels of BC in the particles. Thus recording the EPR spectrum of the particles present in the marine boundary layer and collected on a paper filter yielded direct information on the occurrence of BC. The results for samples together with a blank filter are listed in Table 1.

[17] Six samples have lower relative electron spin resonance (ESR) intensities than the blank filter, indicating undetectable levels of BC in these samples. The other nine samples have relatively higher intensities with a maximum value at 762. The relation between the extent of impact of ship emissions (represented by the F1 factor score determined from inorganic chemical analyses of the filters by *Xie et al.,* 2006) and the level of BC is shown in Figure 7. This result clearly suggests that the occurrence of BC is significantly correlated with ship emissions except for one outlier and the six samples that are below detection limits. In a previous report [*Xie et al.*, 2006], we documented the wind directions and speeds during each of the sampling periods and evaluated the relationship between the frequency of relative wind directions and potential contamination by emission directly from the *Xuelong* research vessel. The lack of correlation between the F1 factor (derived from ship

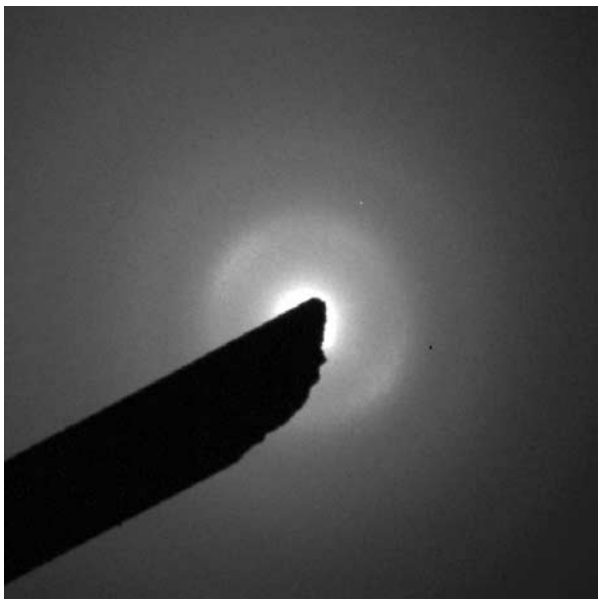

Figure 4. Selected area electron diffraction (SAED) patterns of char particles, indicating an amorphous solid.

emissions) and the frequency of relative wind directions [*Xie et al.*, 2006] suggested that there was no significant contamination from the research vessel and that instead the F1 chemical constituents and the BC were derived from the regional effect of ship emissions.

[18] On the basis of the qualitative analysis of levels of BC, the spatial distribution of BC in the marine boundary layer was estimated and is shown in Figure 8. The relative EPR was normalized by sample volume and a contour plot was drawn utilizing Origin 7.5 (OriginLab Corporation, Northampton, Massachusetts, United States) software. The computation is based on the kriging method, which is appropriate for points with a heterogeneous spatial distribution. This method computes values for each cell in the regular matrix from the values of the points in adjoining cells in the matrix [*John*, 1986]. The contour distribution of BC has several distinct characteristics: (1) the highest levels

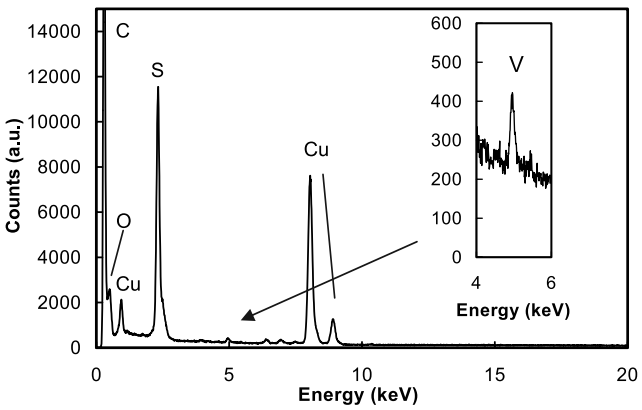

Figure 5. TEM/energy-dispersive X-ray spectroscopy (EDS) spectrum of char particles (copper peak derived from the TEM copper grip), with sulfur and vanadium peaks labeled.

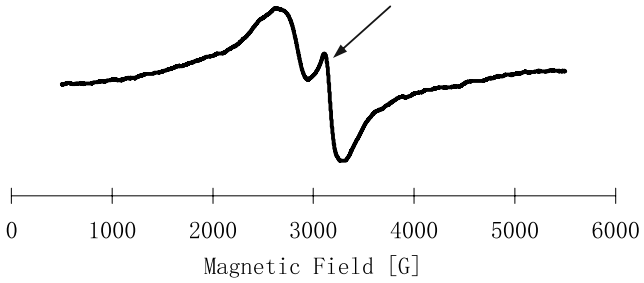

Figure 6. A typical room temperature (T = 300 K) electron paramagnetic resonance (EPR) spectrum of aerosol particles collected in the marine boundary layer. The signal corresponding to black carbon (BC) is shown by the arrow.

of BC occur mostly around the periphery of the Arctic Ocean, (2) the levels of BC decrease from the directions of Russia, Canada, and Alaska toward the central Arctic Ocean, and (3) the maximum levels of BC are present in the Canadian Arctic, including the Beaufort Sea. The spatial distribution seems to correspond to the shipping activities in the Arctic Ocean. In the Russian Arctic, year-round navigation is possible and there is extensive shipping activity. A fleet of ice-strengthened freighters serviced by icebreakers carries cargo of several million tons annually to and from the ports of Murmansk and Vladivostok. In the Canadian Arctic, shipping activities are largely related to the transportation of crude oil. The preferred mode of transportation in the Beaufort Sea, Northwest Passage and Hudson Bay is by tug boat and barge. There are also deliveries of general cargo and petroleum products to eastern Arctic communities. This finding regarding summertime carbonaceous particles, adds important information to the understanding of the characteristics of BC at low altitude in the Arctic.

[19] Recently, *Koch and Hansen* [2005] estimated the different contributions of sources of the Arctic BC from low and high altitudes. The BC related to 'Arctic haze' during the winter and spring was confined to lower altitudes. It has been suggested that at high altitudes BC particles are dominated by south Asian pollution sources. For example, isentropic air mass back trajectories for 7 years of data at Barrow, Alaska showed that during the Arctic haze season, transport from north central Russia occurs near the surface with about 20% frequency, and less frequent (10%) transport from Europe occurs at higher altitude [*Harris and Kahl*, 1994]. With less soluble gaseous pollutants, particulates are more likely to be deposited (mostly rained out) when they are confined to the lower troposphere, as emissions from Europe and Russia commonly are. Over 30% frequency of transport originates from the North Pacific, at altitudes of 1500–3000 m, which is derived from south Asia and includes large amounts of BC emissions. BC also has a relatively large source from tropical biomass burning, again weighting its global emissions southward. Particles from East Asia are more readily lofted to higher altitudes where they can travel greater distances above precipitating clouds. These distant sources are substantial contributors to the Arctic and are expected in high-altitude haze. Such higher-altitude pollution is not limited to the winter/spring, but also appears later in the year as summertime haze, which is often not visible from the surface because of the frequent presence of low-level clouds during summer. Some areas of the Arctic have distinct layers of high BC concentration, often with substantial levels in the free troposphere. For example, BC in aircraft observations over Barrow increased by a factor of 3 above the boundary layer [*Rosen and Hansen*, 1984]. BC from ship emissions may not reach high altitude in summer because of the role of precipitation and the frequent presence of low-level clouds. Thus this source of BC may play an important role only at low altitude.

3.3. Polycyclic Aromatic Hydrocarbons (PAHs)

[20] The 16 PAHs designated by the United States Environmental Protection Agency (US EPA) were detected in extracts from the filters and are listed in Table 2. There are abundant high molecular weight (HMW) compounds, composed of about 80% of the total PAHs, almost 4 times higher than the abundance of low molecular weight (LMW) compounds. The most abundant congener is fluoranthene (HMW) with a value of 0.481 ± 0.723 ng/cm^2 (n = 15), and the least abundant congener is acenaphthylene (LMW) (0.009 ± 0.007 ng/cm^2, n = 15). The relationships between

Table 1. Basic Information for Samples and Electron Spin Resonance (ESR) Intensity

Sample	Latitude(N)	Longitude(W)	Intensity	Fe(×1000)[a]	F1Score[a]	Volume(m^3)
AA-14	73.4	168.8	258	0.6	−0.357	1449
AA-17	71.6	154.4	408	1.23	0.198	1449
AA-18	71.1	161.5	89	0.25	−0.633	1440
AA-19	69.2	168.1	394	0.29	−0.210	1448
AA-27	74.5	156.7	0	0.52	−0.257	1638
AA-28	76.6	153.9	0	0.78	−0.277	1512
AA-29	77.9	150.5	197	0.29	−0.749	3023
AA-30	78.4	148.3	742	0.12	2.424	2235
AA-31	79.9	147.4	367	0.65	−0.093	1512
AA-32	79.8	149.3	114	0.38	−0.601	1638
AA-33	78.9	149.0	261	0.6	−0.622	3024
AA-35	78.7	145.7	712	0.15	2.227	3023
AA-36	78.7	144.7	762	0.84	0.342	3023
AA-38	78.1	152.6	132	0.33	−0.641	2268
AA-39	76.8	166.4	277	0.23	−0.752	3025
Blank filter			252			

[a]From *Xie et al.* [2006].

total PAHs and the congeners, and the levels of BC are also listed in Table 2. With the exception of one congener (naphthalene, which may be an outlier because of its high volatility) total PAHs and the 15 congeners showed significant correlation with the levels of BC. Correlation coefficients range from 0.526 and 0.811, implying that the dominant sources for PAHs may be derived from residual oil combustion by ships.

[21] The current state of knowledge concerning the nature and magnitude of marine emissions is far behind land-based sources, especially concerning "real world" emissions data. This is illustrated by investigations of PAH, polychlorinated biphenyls (PCBs), polychlorinated dibenzodioxins and furans (PCDD/F), and heavy metal emissions, all of which have received considerable attention from land-based sources [*Cooper et al.*, 1996]. Only a few measurement programs have been conducted at sea to provide realistic assessments of air pollution from shipping [*Lloyd's Register Engineering Services*, 1990, 1991, 1993, 1995; *Cooper et al.*, 1996]. *Cooper et al.* [1996] reported hydrocarbon emissions from ferries on the basis of speciation measurements that were carried out on board two passenger ferries (with medium speed, four-stroke diesel engines) operating in the Skagerak-Kattegatt-Oresund region. The results suggested that the levels of PAH emitted from ships are of significance. The total PAH group accounts for about 1.0% of total hydrocarbon emissions.

[22] The levels of persistent organic pollutants (POPs) in the arctic environment have received intensive attention recently. For example, as part of the Canadian commitment to assessing the occurrence, levels, and pathways of POPs to this region, a multiyear systematic air sampling study was established as part of the Northern Contaminants Program [*Halsall et al.*, 1997]. PAHs are one important group of POPs. They are produced from both anthropogenic and natural sources (petrogenic/biogenic). The influence of these source types has been estimated through the analysis of sediments taken from the Beaufort and Barents Sea (Arctic Ocean) [*Yunker et al.*, 1996]. Long-range atmospheric transport from southerly source regions in Eurasia and North America have been presumed to be among the key sources [*Patton et al.*, 1991]. Deposition trends of PAHs, evaluated from cores taken from the Greenland ice cap in the Arctic, have shown a dramatic increase in concentrations over the last 100 years that correlate well with the historical record of world petroleum production [*Halsall et al.*, 1997].

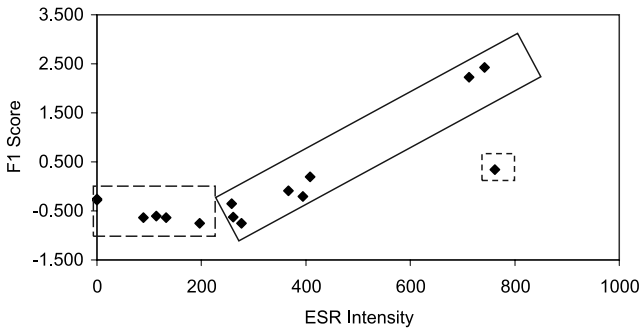

Figure 7. Relationship between the levels of BC (represented by electron spin resonance (ESR) intensity) and the degree of ship contamination (represented by F1 score).

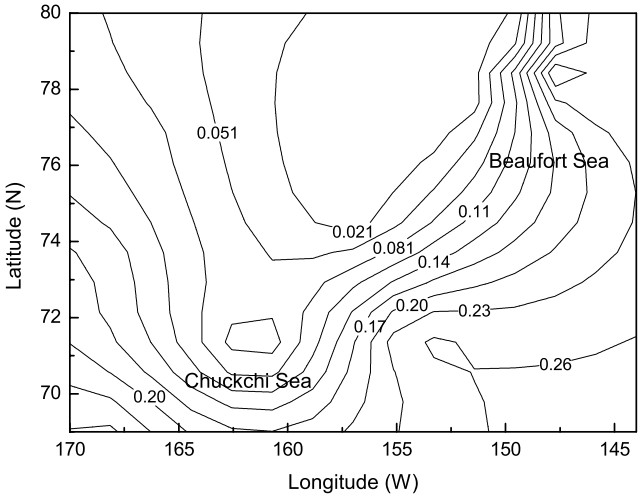

Figure 8. Spatial distribution of BC, which is concentrated around the periphery of the Arctic Ocean.

[23] *Halsall et al.* [1997] investigated the levels of PAHs in the Arctic atmosphere via three land-based locations in the Canadian and Russian Arctic from 1992–1994. The mean value of total PAH concentration (sum of 16 compounds designated by US EPA) ranged from 249 to 508 pg/m^3. There are clear seasonal variations in concentrations. During the colder months of October–April that coincide with the arctic haze period, mean PAHs levels ranged from 312 to 2580 pg/m^3, whereas during the warmer months the mean PAHs levels ranged between 53 and 210 pg/m^3. In our analyses the total PAHs ranged from 142 to 2672 pg/m^3 with a mean value of 702 pg/m^3 (Figure 9). Five samples have levels of PAHs lower than 210 pg/m^3 and the other 11 samples have higher levels of PAHs. The highest value is similar to the one observed in the colder months. Higher levels of PAHs in the warmer months suggest that ship emissions increase the levels of PAHs in the marine boundary of the Arctic Ocean in summer. This results in some important environment concerns. Since PAHs are persistent and accumulate in fat layers of seals and birds [*Cooper et al.*, 1996] the contributions from this source should be further evaluated. Further investigation should also focus on the contribution of the other POPs including chlorobenzenes (e.g., PCB), dioxins and furans. These kinds of POPs were not measured in this study but it has been reported that these compounds can also be emitted by ship combustion [*Cooper et al.*, 1996].

4. Conclusion

[24] Summertime carbonaceous aerosols collected in the marine boundary of the Arctic Ocean were found to be contaminated by ship emissions. The dominant type of carbonaceous particles were char particles, which are a type of black carbon (BC) that has a spherical shape, porous structure and high sulfur content, and which is typically derived from residual oil combustion by ships. The distribution of BC from ship emissions was found to be concentrated around the periphery of the Arctic Ocean, possibly

Table 2. Levels of Polycyclic Aromatic Hydrocarbons (PAHs) Congener and Total PAHs Detected in the Samples (pg/cm^2)

Compounds	aa-14	aa-17	aa-18	aa-19	aa-27	aa-28	aa-29	aa-30	aa-31	aa-32	aa-33	aa-35	aa-36	aa-38	aa-39	ESR[a]
1	165.8	50.7	112.8	121.1	105.8	141.4	251.0	101.3	76.8	141.4	122.9	156.3	211.0	74.4	111.7	0.131
2	6.7	4.3	20.3	17.0	14.7	18.2	50.6	60.5	8.5	17.4	10.7	92.6	52.3	19.8	19.8	0.662
3	6.7	1.4	9.0	9.6	5.1	9.4	12.3	29.0	2.2	9.1	3.7	16.6	14.1	4.8	5.8	0.601
4	23.4	6.1	33.3	45.1	23.5	36.8	66.7	162.4	16.8	31.7	19.7	286.6	142.9	31.8	36.6	0.748
5	108.2	30.1	114.2	167.0	107.7	120.0	686.9	1093.3	79.7	119.4	85.8	1968.3	956.2	127.5	232.6	0.744
6	10.9	2.2	7.2	11.0	8.6	5.6	39.7	69.9	5.1	10.7	11.4	142.6	83.5	7.0	12.6	0.770
7	37.8	12.8	30.6	61.4	35.5	40.5	1519.7	1870.7	138.2	78.6	95.7	1923.5	1097.0	93.1	186.1	0.706
8	27.2	12.2	21.9	49.4	24.8	26.9	962.6	918.1	130.4	69.4	88.0	1193.4	893.8	79.4	187.5	0.720
9	43.7	23.2	7.5	72.0	13.8	5.4	437.1	587.5	133.0	31.4	247.2	330.4	1005.9	55.0	72.3	0.748
10	59.7	53.9	19.0	182.1	35.2	15.8	783.2	1668.8	321.8	85.8	508.3	857.8	1517.9	283.8	233.8	0.811
11	72.0	55.4	15.0	106.4	20.0	6.7	651.5	1742.2	160.5	80.5	458.7	635.0	1077.6	49.1	88.8	0.766
12	68.5	32.0	10.7	38.1	13.4	4.8	334.9	623.8	84.3	44.8	280.8	241.0	513.1	20.0	36.8	0.740
13	77.0	61.4	15.7	58.7	10.2	7.2	95.8	89.9	30.1	97.0	340.8	98.6	800.2	13.3	54.6	0.526
14	116.2	93.4	34.2	177.0	27.5	8.6	917.3	1849.6	267.7	201.6	915.0	498.9	1470.7	46.2	147.0	0.708
15	25.3	11.4	3.4	15.2	3.0	1.0	22.2	75.5	10.7	7.5	67.4	26.6	80.2	5.4	9.0	0.716
16	59.7	60.3	29.0	131.8	15.5	4.8	691.5	1000.2	195.4	155.2	604.2	293.1	748.3	25.8	102.4	0.642
Sum	321.6	94.9	296.8	370.9	265.4	331.5	1107.2	1516.3	189.1	329.8	254.1	2663.0	1460.0	265.4	419.2	0.796

[a]The column data for ESR show the correlation coefficient (R) with PAHs. The compounds are (1) Naphthalene, (2) Acenaphthene, (3) Acenaphthylene, (4) Fluorene, (5) Phenanthrene, (6) Anthracene, (7) Fluoranthene, (8) Pyrene, (9) Benzo[a]anthracene, (10) Chrysene, (11) Benzo[b]fluoranthene, (12) Benzo[k]fluoranthene, (13) Benzo[a]pyrene, (14) Indeno[123-cd]pyrene, (15) Dibenzo[a,h]anthracene, and (16) and Benzo[ghi]pyrene, respectively.

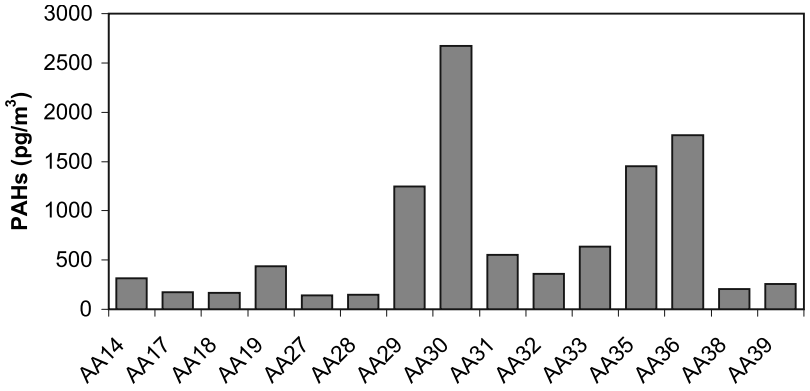

Figure 9. Levels of polycyclic aromatic hydrocarbons (PAHs), ranging from 142 to 2672 pg/m^3 (mean = 702 pg/m^3).

representing more intense contamination by ships around the Russian and Canadian Arctic coasts. The abundance of PAHs were measured on BC particles. The levels of PAHs ranged from 142 to 2672 pg/m^3 (mean = 702 pg/m^3), significantly higher than the previous values measured by land-based observation. Since ship contamination was demonstrated to be a regional phenomenon and not contamination from the research vessel itself, this kind of source may result in some environmental concerns (e.g., levels of POPs) that have not been received previous attention.

[25] **Acknowledgments.** This study was supported by grants to Z. Xie from the China National Natural Science Foundation (40306001), the Foundation for the Author of National Excellent Doctoral Dissertation of P. R. China (200354) from the Ministry of Education of China, and the Chinese Academy of Sciences. Additional support was provided by the U.S. National Science Foundation (ARC-0435893) to J. Blum and by NSF/NIRT (EAR-0403732) to R. Ewing. We thank N. Yordanov and M. Posfai for helpful discussions and for providing related references and two anonymous reviewers for their critical and constructive comments.

References

Ackerman, A., O. Toon, D. Stevens, A. Heymsfield, V. Ramanathan, and E. Welton (2000), Reduction of tropical cloudiness by soot, *Science*, *288*, 1042–1047.

Charlson, R. J., S. E. Schwartz, J. M. Hales, R. O. Cess, J. A. Coakley Jr., J. E. Hansen, and D. J. Hofman (1992), Climate forcing by anthropogenic aerosols, *Science*, *255*, 423–430.

Chen, Y. Z., N. Shah, F. E. Huggins, and G. P. Huffman (2004), Investigation of the microcharacteristics of $PM_{2.5}$ in residual oil fly ash by analytical transmission electron microscopy, *Environ. Sci. Technol.*, *38*, 6553–6560.

Chen, Y. Z., N. Shah, A. Rraun, F. E. Huggins, and G. P. Huffman (2005), Electron microscopy investigation of carbonaceous particulate matter generated by combustion of fossil fuels, *Energy Fuels*, *19*, 1644–1651.

Cheng, M. D., P. K. Hopke, L. Barrie, A. Rippe, M. Olson, and S. Landsberger (1993), Qualitative determination of source regions of aerosol in Canadian high Arctic, *Environ. Sci. Technol.*, *27*, 2063–2071.

Chughtai, A. R., G. R. Williams, M. M. O. Atteya, N. J. Miller, and D. M. Smith (1999), Carbonaceous particle hydration, *Atmos. Environ.*, *33*, 2679–2687.

Chughtai, A. R., J. M. Kim, and D. M. Smith (2002), The effects of air/fuel ratio on properties and reactivity of combustion soots, *J. Atmos. Chem.*, *43*, 21–43.

Clarke, A. D., and J. Noone (1985), Measurements of soot aerosol in Arctic snow, *Atmos. Environ.*, *19*, 2045–2054.

Cooke, W. F., and J. J. N. Wilson (1996), A global black carbon aerosol model, *J. Geophys. Res.*, *101*, 19,395–19,409.

Cooper, D. A., K. Peterson, and D. Simpson (1996), Hydrocarbon, PAH and PCB emissions from ferries: A case study in the Skagerak-Kattegatt-Oresund region, *Atmos. Environ.*, *30*, 2463–2473.

Crimmins, B. S., R. R. Dickerson, B. G. Doddridge, and J. E. Baker (2004), Particulate polycyclic aromatic hydrocarbons in the Atlantic and Indian Ocean atmospheres during the Indian Ocean Experiment and Aerosols99: Continental sources to the marine atmosphere, *J. Geophys. Res.*, *109*, D05308, doi:10.1029/2003JD004192.

Douglas, W., D. W. Dockery, A. Pope III, X. Xu, J. D. Spengler, J. H. Ware, M. E. Fey, B. G. Ferris, and F. E. Speizer (1993), An association between air pollution and mortality in six US cities, *N. Engl. J. Med.*, *329*, 1753–1759.

Fernandes, M., and P. Brooks (2003), Characterization of carbonaceous combustion residues: II. Nonpolar organic compounds, *Chemosphere*, *53*, 447–458.

Fernandes, M. B., J. O. Skjemstad, B. B. Johnson, J. D. Wells, and P. Brooks (2003), Characterization of carbonaceous combustion residues. I. Morphological, elemental and spectroscopic features, *Chemosphere*, *51*, 785–795.

Halsall, C. J., L. A. Barrie, P. Fellin, D. C. G. Muir, B. N. Billeck, L. Lockhart, F. Y. Rovinsky, E. Y. Konnonoy, and B. Pastukhov (1997), Spatial and temporal variation of polycyclic aromatic hydrocarbons in the Arctic atmosphere, *Environ. Sci. Technol.*, *31*, 3593–3599.

Hansen, J., and L. Nazarenko (2004), Soot climate forcing via snow and ice albedos, *Proc. Natl. Acad. Sci. U. S. A.*, *101*, 423–428, doi:10.1073/pnas.2237157100.

Hansen, J., M. Sato, and R. Ruedy (1997), Radiative forcing and climate response, *J. Geophys. Res.*, *102*, 6831–6864.

Harris, J. M., and J. D. W. Kahl (1994), Analysis of 10-day isentropic flow patterns for Barrow, Alaska: 1985–1992, *J. Geophys. Res.*, *99*, 25,845–25,855.

Haywood, J. M., and V. Ramaswamy (1998), Global sensitivity studies of the direct radiative forcing due to anthropogenic sulfate and black carbon aerosols, *J. Geophys. Res.*, *103*, 6043–6058.

John, D. C. (1986), *Statistics and Data Analysis in Geology*, 2nd ed., 383 pp., John Wiley, Hoboken, N. J.

Jones, C. C., A. R. Chughtai, B. Murgugaverl, and D. M. Smith (2004), Effects of air/fuel combustion ratio on the polycyclic aromatic hydrocarbon content of carbonaceous soots from selected fuels, *Carbon*, *42*, 2471–2484.

Kirchner, V., V. Scheer, and R. Vogt (2000), FTIR spectroscopic investigation of the mechanism and kinetics of the heterogeneous reactions of NO_2 and HNO_3 with soot, *J. Phys. Chem. A.*, *104*, 8908–8915.

Koch, D., and J. Hansen (2005), Distant origins of Arctic black carbon: A Goddard Institute for Space Studies ModelE experiment, *J. Geophys. Res.*, *110*, D04204, doi:10.1029/2004JD005296.

Lloyd's Register Engineering Services (1990), *Marine Exhaust Emissions Research Programme, Phase I Steady-State Operation*, London.

Lloyd's Register Engineering Services (1991), *Marine Exhaust Emissions Research Programme, Phase I Steady-State Operation: Slow Speed Addendum*, London.

Lloyd's Register Engineering Services (1993), *Marine Exhaust Emissions Research Programme, Phase II: Transient Emission Trials*, London.

Lloyd's Register Engineering Services (1995), *Marine Exhaust Emissions Research Programme*, London.

Lowenthal, D. H., and R. D. Borys (1997), Sources of pollution aerosol at Dye 3, Greenland, *Atmos. Environ.*, *22*, 3707–3717.

Lowenthal, D. H., and K. A. Rahn (1985), Regional sources of pollution aerosol at Barrow, Alaska during winter 1979–80 as deduced from elemental tracers, *Atmos. Environ.*, *19*, 2011–2024.

Novakov, T., S. Menon, T. W. Kirchstetter, D. Koch, and J. E. Hanse (2005), Aerosol organic carbon to black carbon ratios: Analysis of published data and implications for climate forcing, *J. Geophys. Res.*, *110*, D21205, doi:10.1029/2005JD005977.

Ochsenkuhn-Petropoulou, M., K. Staikos, G. Matuschek, and A. Kettrup (2003), On-line determination of polycyclic aromatic hydrocarbons in airborne particulate matter by using pyrolysis/GC-MS, *J. Anal. Appl. Pyrolysis*, *70*, 73–85.

Patton, G. W., M. D. Walla, T. F. Bidleman, and L. A. Barrie (1991), Polycyclic aromatic and organochlorine compounds in the atmosphere of northern Ellesemere-Island, Canada, *J. Geophys. Res.*, *96*, 10,867–10,877.

Penner, J. E., H. Eddleman, and T. Novakov (1993), Towards the development of a global inventory for black carbon emissions, *Atmos. Environ.*, *27*, 1277–1295.

Pope, C. A., III, R. L. Venier, E. G. Lovett, A. C. Larson, M. E. Raizenne, R. E. Kanner, J. Schwartz, G. M. Villegas, D. R. Gold, and D. W. Dockery (1999), Heart rate variability associated with particulate air pollution, *Am. Heart J.*, *138*, 890–899.

Rahn, K. A., and D. H. Lowenthal (1984), Elemental tracers of distant regional pollution aerosols, *Science*, *223*, 132–139.

Rosen, H., and A. D. A. Hansen (1984), Role of combustion-generated carbon particles in the absorption of solar radiation in the Arctic haze, *Geophys. Res. Lett.*, *11*, 461–464.

Shaw, G. E. (1995), The Arctic haze phenomenon, *Bull. Am. Meteorol. Soc.*, *76*, 2403–2413.

Utsunomiya, S., and R. C. Ewing (2003), Application of high-angle annular dark field scanning transmission electron microscopy (HAADF-STEM), STEM-energy dispersive X-ray spectrometry (EDX), and energy-filtered (EF)-TEM to the characterization of nanoparticles in the environment, *Environ. Sci. Technol.*, *37*, 786–791.

Utsunomiya, S., K. A. Jensen, G. J. Keeler, and R. C. Ewing (2002), Uraninite and fullerene in atmospheric particulates, *Environ. Sci. Technol.*, *36*, 4943–4947.

Xie, Z. Q., L. G. Sun, J. J. Wang, and B. Z. Liu (2002), A potential source of atmospheric sulfur from penguin colony emissions, *J. Geophys. Res.*, *107*(D22), 4617, doi:10.1029/2002JD002114.

Xie, Z. Q., X. M. Wang, L. G. Sun, N. Y. Long, and B. B. Cheng (2005), Characteristics of carbonaceous aerosol in a two-week campaign at Ny-Alesund, *Chin. J. Polar Sci.*, *16*, 101–108.

Xie, Z. Q., L. G. Sun, J. D. Blum, Y. Y. Huang, and W. He (2006), Summertime aerosol chemical components in the marine boundary layer of the Arctic Ocean, *J. Geophys. Res.*, *111*, D10309, doi:10.1029/2005JD006253.

Yordanov, N. D., and I. Najdenova (2004), Selective estimation of soot in home dust by EPR spectrometry, *Spectrochim. Acta A Mol. Biomol. Spectrosc.*, *60*, 1367–1370.

Yordanov, N. D., B. Veleva, and R. Christov (1996), EPR study of aerosols with carbonaceous products in the urban air, *Appl. Magn. Reson.*, *10*, 439–445.

Yordanov, N. D., S. Lubenova, and S. Sokolova (2001), On the possibility for separate determination of pyrolyzed products (soot and polycyclic aromatic hydrocarbons) in aerosols by EPR spectrometry, *Atmos. Environ.*, *35*, 827–831.

Yunker, M. B., L. R. Snowdon, R. W. MacDonald, J. N. Smith, M. G. Fowler, D. N. Skibo, F. A. McLaughlin, A. I. Danyushevskaya, V. I. Petrova, and G. I. Ivanov (1996), Polycyclic aromatic hydrocarbon composition and potential sources for sediment samples from the Beaufort and Barents Seas, *Environ. Sci. Technol.*, *30*, 1310–1320.

J. D. Blum, R. C. Ewing, S. Utsunomiya, and Z. Xie, Department of Geological Sciences, University of Michigan, Ann Arbor, MI 48109, USA. (zqxie@umich.edu)

L. Sun, Institute of Polar Environment, School of Earth and Space Sciences, University of Science and Technology of China, Hefei, Anhui, 230026, China.

X. Wang, State Key Laboratory of Organic Geochemistry, Guangzhou Institute of Geochemistry, Chinese Academy of Sciences, Wushan, Guangzhou, 510640, China.